Observation of Nearly Perfect Irrotational Flow in Normal and Superfluid Strongly Interacting Fermi Gases

Bason Clancy, Le Luo, and John E. Thomas*

Duke University, Department of Physics, Durham, North Carolina, 27708, USA

(Received 31 May 2007; published 1 October 2007)

We study the hydrodynamic expansion of a rotating strongly interacting Fermi gas by releasing a cigar-shaped cloud with a known angular momentum from an optical trap. As the aspect ratio of the expanding cloud approaches unity, the angular velocity increases, indicating quenching of the moment of inertia I to as low as 0.05 of the rigid body value I_{rig}. Remarkably, we observe this behavior in both the superfluid and collisional normal fluid regimes, which obey nearly identical zero-viscosity irrotational hydrodynamics. We attribute irrotational flow in the normal fluid to a decay of the rotational part of the stream velocity during expansion, which occurs when the shear viscosity is negligible. Using conservation of angular momentum, we directly observe a fundamental result of irrotational hydrodynamics, $I/I_{\mathrm{rig}} = \delta^2$, where δ is the deformation parameter of the cloud.

DOI: 10.1103/PhysRevLett.99.140401 PACS numbers: 03.75.Ss, 32.80.Pj

Strongly interacting Fermi gases [1] provide a unique paradigm for exploring strongly interacting fluids in nature, such as high temperature superfluids and exotic normal fluids including the quark-gluon plasma of the big bang [2,3] or minimum viscosity strongly interacting fields [4]. Strongly interacting Fermi gases exhibit hydrodynamic flow not only in the superfluid regime, but also in the normal regime where the origin of nearly perfect hydrodynamics is of great interest [5]. For superfluids, a well-known requirement is irrotational hydrodynamics, i.e., $\nabla \times \mathbf{v} = 0$, which is a consequence of the macroscopic wave function. However, for the normal fluid, perfect irrotational flow is not required or expected.

In this Letter, we study the hydrodynamic expansion of a rotating strongly interacting Fermi gas of ^{6}Li atoms. We release a cigar-shaped cloud with a known angular momentum L from an optical trap, and measure the angular velocity Ω about the y axis and the aspect ratio of the principal axes (z, x) from the time-of-flight images. The data are in excellent agreement with irrotational hydrodynamics [6–8] in the superfluid regime, and surprisingly in the normal fluid regime as well. Conservation of angular momentum enables a model-independent measurement of the effective moment of inertia $I \equiv L/\Omega$. We find that I is suppressed with respect to the rigid body value, I_{rig}, directly testing a fundamental prediction of irrotational flow [6],

$$I/I_{\mathrm{rig}} = \delta^2 \equiv \langle z^2 - x^2\rangle^2/\langle z^2 + x^2\rangle^2, \qquad (1)$$

where the deformation parameter δ and I_{rig} are obtained from the cloud images.

Previously, the hydrodynamics of a strongly interacting Fermi gas with zero angular momentum has been observed in expansion [1,9,10] and in collective modes [11–14]. Vortex lattices have been used to demonstrate superfluidity in a strongly interacting Fermi gas [15,16].

In our experiments, a degenerate strongly interacting Fermi gas is prepared by all-optical methods [1]. We employ a 50:50 mixture of the two lowest hyperfine states of ^{6}Li atoms in a bias magnetic field near a broad Feshbach resonance at 834 G [17]. After evaporation, the trap depth is recompressed to $U_0/k_B = 100\ \mu$K, which is large compared to the energy per particle of the gas.

At the final trap depth U_0, the measured oscillation frequencies in the transverse directions are $\omega_x = 2\pi \times 2354(4)$ Hz and $\omega_y = 2\pi \times 1992(2)$ Hz, while the axial frequency is $\omega_z = 2\pi \times 71.1(.3)$ Hz, producing a cigar-shaped trap with $\omega_z/\omega_x = 0.032$. The total number of atoms N typically is 1.3×10^5. The corresponding Fermi energy E_F for an ideal (noninteracting) harmonically trapped gas at the trap center is $E_F = \hbar(3N\omega_x\omega_y\omega_z)^{1/3} = 2.4\ \mu\mathrm{K}\ k_B$.

Samples with energies well above the ground state are prepared either by reducing the forced evaporation time or, starting from near the ground state, by adding energy using release and recapture. The cloud is held for 0.5 s to assure equilibrium. The total energy E of the cloud is determined in the universal, strongly interacting regime from the mean square axial (z) cloud size, using $E = 3m\omega_z^2\langle z^2\rangle$, where m is the atom mass [18,19].

Once the trapped gas has been prepared in the desired energy state, the trap is suddenly rotated as shown in Fig. 1.

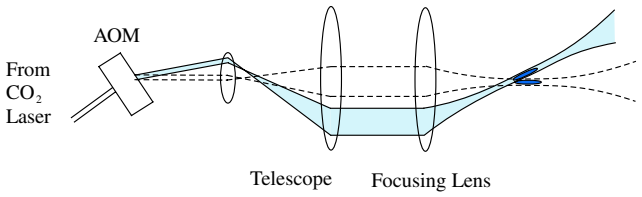

FIG. 1 (color online). Scheme to rotate the optical trap by changing the frequency of an AOM.

Rotation of the trap CO_2 laser beam is accomplished by changing the frequency of the acousto-optic modulator (AOM) that controls the trap laser intensity, using a radio frequency (rf) switch. When the frequency is changed, the position of the beam on the final focusing lens translates. This translation causes primarily a rotation of the cigar-shaped trap at the focal point, about an axis (y) perpendicular to the plane of the cigar-shaped trap. A scissors mode [20] is excited by the rotation. Then the cloud is permitted to oscillate in the trap for a chosen period that determines the initial angular velocity of the cloud before release.

Figure 2 shows cloud images as a function of expansion time for the coldest samples, with a typical energy $E = 0.56E_F$ near the ground state [18]. When the gas is released without rotation of the trap, Fig. 2 (top), the Fermi cloud expands anisotropically, as previously predicted [21] and observed [1,9]. In that case, the gas expands rapidly in the narrow (x, y) directions of the cigar, while remaining nearly stationary in the long (z) direction, inverting the aspect ratio σ_x/σ_z as the cloud becomes elliptical in shape.

Quite different expansion dynamics occurs when the cloud is rotating prior to release, Fig. 2 (middle) and (bottom). In this case, the aspect ratio σ_x/σ_z initially increases toward unity. However, as the aspect ratio approaches unity, the moment of inertia decreases and the angular velocity of the principal axes increases to conserve angular momentum as previously predicted [6] and observed [7,8] in a superfluid Bose-Einstein condensate (BEC). After the aspect ratio reaches a maximum less than unity [6], it and the angular velocity begin to decrease as the angle of the cigar-shaped cloud approaches a maximum value less than 90°.

Figure 3 shows the measured aspect ratio and the angle of the principal axes versus expansion time, which are determined from the cloud images. The measured density profiles are fit with a two-dimensional Gaussian distribution, which takes the form $A\exp[-a\tilde{z}^2 - b\tilde{z}\,\tilde{x} - c\tilde{x}^2]$, where $\tilde{z}$, $\tilde{x}$ are laboratory coordinates. From the values of a, b, and c, the aspect ratio of the rotated cloud and the angle of the long z axis of the cloud with respect to the laboratory $\tilde{z}$ axis are determined.

We attempt to model the data for measurements near the ground state (blue solid circles and green triangles of Fig. 3), by using a zero temperature hydrodynamic theory for the expansion of a rotating strongly interacting Fermi gas in the superfluid regime. A theory of this type was first used to describe the rotation and expansion of a weakly interacting BEC [6,22]. The model consists of the Euler and continuity equations for a superfluid, where the velocity field $\mathbf{v}$ is irrotational, i.e., $\nabla \times \mathbf{v} = 0$. The driving force for the expansion arises from the gradient of the chemical potential, which we take to be that of a strongly interacting Fermi gas [1,23]. We also include the force arising from magnet field curvature, which changes the angular momentum at the point of maximum aspect ratio by 10% and the angle and aspect ratio at the longest release times by a few percent. To determine the initial conditions for our model, we directly measure the initial angular velocity and axial cloud radius just after release, while assuming the transverse radii are given by zero temperature values for our trap frequencies. The results yield excellent agreement with all of the Fermi gas angle and aspect ratio data, with no free parameters, as shown in Fig. 3.

We make a model-independent measurement of the effective moment of inertia $I \equiv L/\Omega$, where Ω is the angular velocity of the principal axes of the cloud after release and $L = \Omega_0 I_0$ is the angular momentum, which is conserved during the expansion (we neglect the small change arising from the magnetic potential). The angular velocity Ω is calculated from the time derivative of a polynomial fit to the angle versus time data. To determine the initial moment of inertia I_0, we note that for a cigar-shaped cloud with a small aspect ratio σ_x/σ_z, the moment of inertia for the irrotational fluid is nearly equal to the rigid body value [6,8]. For our parameters $I_0 \simeq Nm\langle z^2\rangle_0$, within 0.3% accuracy, where $\langle z^2\rangle_0$ is measured from the cloud images. The measured effective moment of inertia

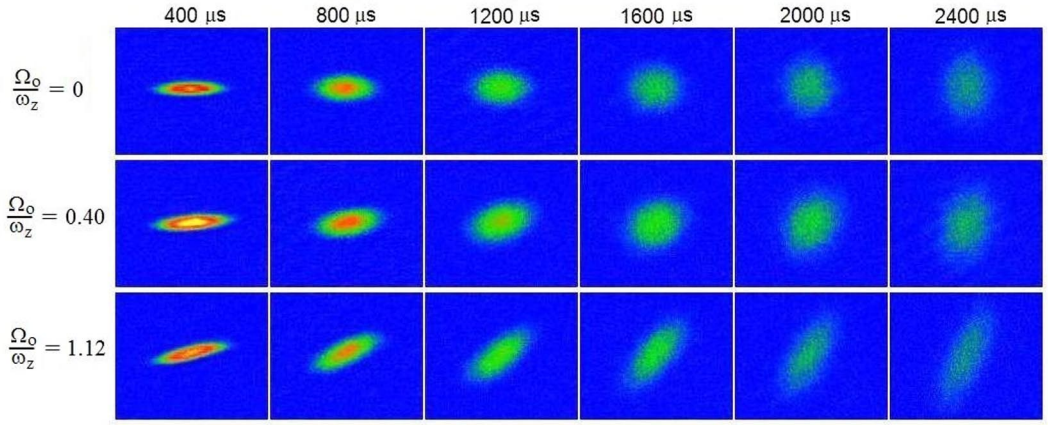

FIG. 2 (color online). Expansion of a rotating, strongly interacting Fermi gas. Ω_0, initial angular velocity; ω_z, trap axial frequency.

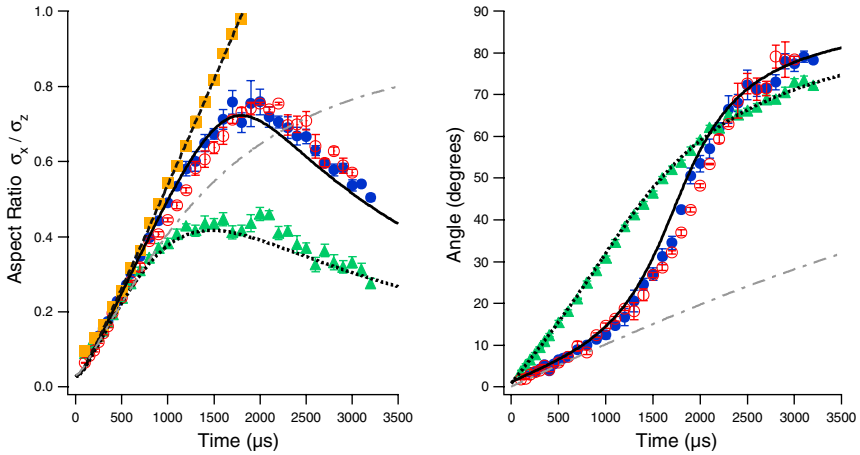

FIG. 3 (color online). Aspect ratio and angle of the principal axis versus time. Orange squares (aspect ratio for $\Omega_0 = 0$); blue solid circles ($\Omega_0/\omega_z = 0.40$, $E/E_F = 0.56$); red open circles ($\Omega_0/\omega_z = 0.40$, $E/E_F = 2.1$); green triangles ($\Omega_0/\omega_z = 1.12$, $E/E_F = 0.56$). The solid, dashed, and dotted lines are the theoretical calculations using the measured initial conditions. The gray dot-dashed line shows the energy-independent predictions for a ballistic gas with $\Omega_0/\omega_z = 0.40$.

after release is then $I = I_0\Omega_0/\Omega$. The corresponding rigid body moment of inertia is determined from the fit to the cloud profile, $I_{\text{rig}} = Nm\langle x^2 + z^2\rangle$. Hence, we obtain $I/I_{\text{rig}} = (\Omega_0/\Omega)I_0/I_{\text{rig}}$.

We note that the measured I generally is not the equilibrium moment of inertia of the rotating cloud, which requires that the velocity fields of the normal and superfluid components reach their steady state values [23]. However, in our highly cigar-shaped trap, whether the system is in equilibrium or not, the initial angular momentum is essentially equal to the rigid body value, independent of the superfluid and normal fluid composition. To see this physically, note that for rotation about the y axis, the initial stream velocity for irrotational flow is $\mathbf{v} = \Omega_0 z\mathbf{i} + \Omega_0 x\mathbf{k}$, while for rotational flow, $\mathbf{v} = \Omega_0 z\mathbf{i} - \Omega_0 x\mathbf{k}$. These differ only for the z components, which are negligible as the aspect ratio σ_x/σ_z tends to zero.

Figure 4 shows the measured minimum value of I/I_{rig} as a function of initial angular velocity Ω_0. The smallest values of I/I_{rig} occur for the smallest Ω_0. For the coldest clouds (blue solid circles), where the energy of the gas is close to that of the ground state, the gas is believed to be in the superfluid regime [11,15,18]. In this case, we observe values of I/I_{rig} as small as 0.05, smaller than those obtained from the scissors mode of a BEC of atoms [24,25]. The solid line shows I/I_{rig} as predicted by the superfluid hydrodynamic theory, which is in very good agreement with the measurements.

Such nearly perfect irrotational flow usually arises only in the superfluid regime. For example, normal weakly interacting Bose gases expand ballistically above the critical temperature. We observe ballistic expansion of the Fermi gas at 528 G, where the scattering length vanishes. In this case, the aspect ratio asymptotically approaches unity, and there is no increase in angular velocity.

In contrast, for a normal strongly interacting Fermi gas, we observe quenching of the moment of inertia. To investigate the normal fluid regime, we increase E to $2.1E_F$, which is well above the transition energy, $E_c = 0.94E_F$ as estimated from the measured change in the behavior of the entropy [18]. At $E = 2.1E_F$, the gas is in the normal regime, as the measured entropy versus energy near $2E_F$ closely coincides with that of an ideal gas [18]. The open red circles in Fig. 3, show the aspect ratio and angle versus time for an initial angular velocity $\Omega_0/\omega_z = 0.4$ and $E = 2.1E_F$. The results for the normal fluid are nearly identical to those obtained for $\Omega_0/\omega_z = 0.4$ in the superfluid regime (blue solid circles).

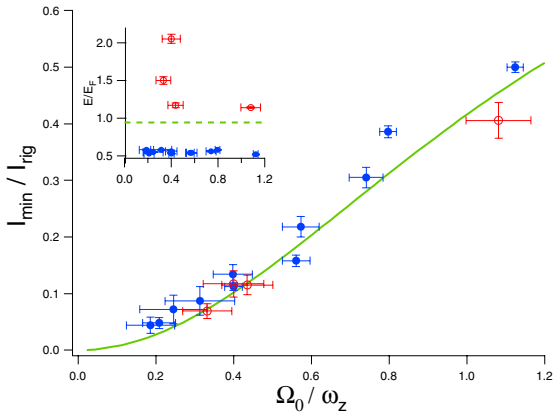

FIG. 4 (color online). Quenching of the moment of inertia versus initial angular velocity Ω_0. $I_{\text{min}}/I_{\text{rig}}$ is the minimum moment of inertia measured during expansion in units of rigid body value. Blue solid circles: initial energy before rotation below the superfluid transition energy $E_c = 0.94E_F$. Red open circles: initial energy above E_c. Green solid line: Prediction for irrotational flow. Inset shows the energy for each data point with the dashed line at E_c.

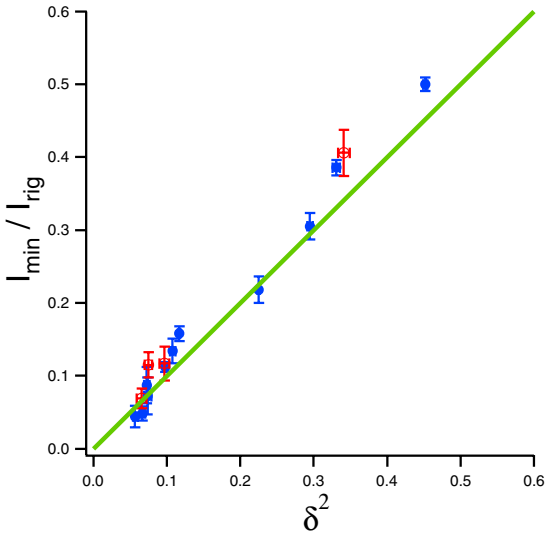

FIG. 5 (color online). Quenching of the moment of inertia versus the square of the measured cloud deformation factor δ. Blue solid circles: initial energy below the superfluid transition energy $E_c = 0.94E_F$. Red open circles: initial energy above E_c. Green solid line: prediction for irrotational flow.

We attribute the observed irrotational flow in the normal strongly interacting fluid to low viscosity collisional hydrodynamics. For release from a harmonic trap, the stream velocity $\mathbf{v}$ is linear in the laboratory coordinates $\tilde{\mathbf{x}}$. Assuming rotation about the y axis, we have $v_{\tilde{x}} = \alpha_x \tilde{x} + (\alpha + \Omega)\tilde{z}$, $v_{\tilde{y}} = \alpha_y \tilde{y}$, $v_{\tilde{z}} = \alpha_z \tilde{z} + (\alpha - \Omega)\tilde{x}$. Here, $\alpha_i(t)$ and $\alpha(t)$ describe the irrotational velocity field and $\Omega(t)$ the rotational part. With zero viscosity, the hydrodynamic equations of motion yield the result $\partial\Omega/\partial t + (\alpha_x + \alpha_z)\Omega = 0$. After release, the stream velocity increases, and α_x becomes the order of ω_x. Hence, Ω decays rapidly, on the time scale $1/\omega_x \ll 1/\Omega,\ 1/\omega_z$. For negligible viscosity, the gas cannot maintain rigid rotation during expansion.

We see from Fig. 4 that the moment of inertia is quenched for energies both above and below the superfluid transition. Irrotational hydrodynamics generally requires the quenched moment of inertia to be given by Eq. (1), where the deformation parameter δ is computed with respect to the principal axes. Figure 5 compares the measured minimum values of I/I_{rigid} with the values of δ^2 obtained from the measured cloud aspect ratios. The data directly verify that this fundamental prediction is valid in both the normal and superfluid regimes of a strongly interacting Fermi gas.

This research was supported by the Chemical Sciences, Geosciences and Biosciences Division of the Office of Basic Energy Sciences, Office of Science, U. S. Department of Energy, and the Physics Divisions of the Army Research Office and the National Science Foundation.

*jet@phy.duke.edu

[1] K. M. O'Hara, S. L. Hemmer, M. E. Gehm, S. R. Granade, and J. E. Thomas, Science **298**, 2179 (2002).
[2] P. F. Kolb and U. Heinz, *Quark Gluon Plasma 3* (World Scientific, Singapore, 2003), p. 634.
[3] E. Shuryak, Prog. Part. Nucl. Phys. **53**, 273 (2004).
[4] P. K. Kovtun, D. T. Son, and A. O. Starinets, Phys. Rev. Lett. **94**, 111601 (2005).
[5] G. M. Bruun and H. Smith, Phys. Rev. A **75**, 043612 (2007); P. Massignan , G. M. Bruun, and H. Smith, Phys. Rev. A **71**, 033607 (2005).
[6] M. Edwards, C. W. Clark, P. Pedri, L. Pitaevskii, and S. Stringari, Phys. Rev. Lett. **88**, 070405 (2002).
[7] G. Hechenblaikner, E. Hodby, S. A. Hopkins, O. M. Maragó, and C. J. Foot, Phys. Rev. Lett. **88**, 070406 (2002).
[8] M. Modugno, G. Modugno, G. Roati, C. Fort, and M. Inguscio, Phys. Rev. A **67**, 023608 (2003).
[9] T. Bourdel, J. Cubizolles, L. Khaykovich, K. M. F. Magãlhaes, S. Kokkelmans, G. V. Shlyapnikov, and C. Salomon, Phys. Rev. Lett. **91**, 020402 (2003).
[10] C. A. Regal and D. S. Jin, Phys. Rev. Lett. **90**, 230404 (2003).
[11] J. Kinast, S. L. Hemmer, M. E. Gehm, A. Turlapov, and J. E. Thomas, Phys. Rev. Lett. **92**, 150402 (2004).
[12] J. Kinast, A. Turlapov, and J. E. Thomas, Phys. Rev. Lett. **94**, 170404 (2005).
[13] M. Bartenstein, A. Altmeyer, S. Riedl, S. Jochim, C. Chin, J. H. Denschlag, and R. Grimm, Phys. Rev. Lett. **92**, 203201 (2004).
[14] A. Altmeyer, S. Riedl, C. Kohstall, M. J. Wright, R. Geursen, M. Bartenstein, C. Chin, J. H. Denschlag, and R. Grimm, Phys. Rev. Lett. **98**, 040401 (2007).
[15] M. Zwierlein, J. Abo-Shaeer, A. Schirotzek, C. Schunck, and W. Ketterle, Nature (London) **435**, 1047 (2005).
[16] C. H. Schunck, M. W. Zwierlein, A. Schirotzek, and W. Ketterle, Phys. Rev. Lett. **98**, 050404 (2007).
[17] M. Bartenstein, A. Altmeyer, S. Riedl, R. Geursen, S. Jochim, C. Chin, J. H. Denschlag, R. Grimm, A. Simoni, E. Tiesinga, C. J. Williams, and P. S. Julienne, Phys. Rev. Lett. **94**, 103201 (2005).
[18] L. Luo, B. Clancy, J. Joseph, J. Kinast, and J. E. Thomas, Phys. Rev. Lett. **98**, 080402 (2007).
[19] J. E. Thomas, J. Kinast, and A. Turlapov, Phys. Rev. Lett. **95**, 120402 (2005).
[20] D. Guéry-Odelin and S. Stringari, Phys. Rev. Lett. **83**, 4452 (1999).
[21] C. Menotti, P. Pedri, and S. Stringari, Phys. Rev. Lett. **89**, 250402 (2002).
[22] A. Recati, F. Zambelli, and S. Stringari, Phys. Rev. Lett. **86**, 377 (2001).
[23] M. Cozzini and S. Stringari, Phys. Rev. Lett. **91**, 070401 (2003).
[24] F. Zambelli and S. Stringari, Phys. Rev. A **63**, 033602 (2001).
[25] O. M. Maragó, G. Hechenblaikner, E. Hodby, S. A. Hopkins, and C. J. Foot, J. Phys. Condens. Matter **14**, 343 (2002).